Articles
doi.org/10.1002/batt.201900173

Chemistry Europe
European Chemical Societies Publishing

Special Collection

Engineering of Sn and Pre-Lithiated Sn as Negative Electrode Materials Coupled to Garnet Ta-LLZO Solid Electrolyte for All-Solid-State Li Batteries

Giulio Ferraresi,*[a] Sven Uhlenbruck,[b] Chih-Long Tsai,[b] Petr Novák,[a] and Claire Villevieille*[a, c]

All-solid-state batteries using garnet-type solid electrolyte are considered as a promising solution for the next generation energy storage systems but to date they still suffer from low ionic conductivity compared to organic liquid electrolytes and poor interfacial contact between the electroactive materials and the electrolyte. Here we propose several proof-of-concept level strategies to enhance the interfacial contact between the electroactive material Sn and the solid electrolyte Ta-LLZO doped (hereafter called LLZTa) to enable proper electrochemical cycling. First, we demonstrate that the conventional slurry-based technique is not appropriate to ensure cycling of a Sn based electrode in all-solid-state batteries due to poor interfacial contact. Then, we demonstrate (proof-of-concept) that thin films deposition is a more suitable approach to ensure electrochemical activity but the large volume changes of Sn during alloying process is leading to a rapid cell failure. This last challenge was overcome by the use of a chemically pre-lithiated Sn thin film which then delivers, after an activation process, specific charge close to the theoretical one (900 mAh/g) at C/30 rate and $T = 80\,^{\circ}C$.

1. Introduction

Li-ion batteries are the most widely used electrochemical energy storage system for portable applications such as laptops and smartphones but also invaded more and more the electric vehicle market.[1] Recently, however, several incidents were reported about thermal runaway and safety concerns of Li-ion batteries pushing researchers to provide alternative and safer solutions.[2] One of them relies on the replacement of the flammable liquid organic electrolyte with a solid one. In recent years, many solid electrolytes belonging to different material families have been investigated as promising candidates for fast Li^+ conducting electrolytes.[3] Clearly, the most suitable candidates have reasonably high ionic conductivities (as close as possible to that of organic electrolytes). In particular, sulfide-based electrolytes (e.g. $Li_{10}GeP_2S_{12}$ and $Li_7P_3S_{11}$) exhibit comparable ionic conductivities to liquid electrolytes.[4] Unfortunately, for these electrolytes with promising ionic conductivities, there are severe concerns regarding i) their extremely narrow electrochemical stability windows and, ii) their safety risks owing to the release of toxic H_2S gas during synthesis and upon exposure to air or moisture. Other candidates are dense ceramic electrolytes that have attracted much interest owing to the possibility of combining relatively high ionic conductivities (for a solid at room temperature) with wide electrochemical stability windows.[5] These materials follow the Arrhenius equation, i.e. their ionic conductivity increases with temperature, which opens new perspectives for all-solid-state batteries based on safe garnet-type solid electrolytes.[6] However, control over the solid electrolyte-solid (active material) interface is crucial because if contact between these components is not optimal, the interfacial resistance can be so high that the battery does not cycle.[7] The interface engineering approach developed by Van den Broek et al.[8] leads to proper cycling of a $Li_4Ti_5O_{12}$ active material at 95 °C, which, so far, has been almost impossible under standard conditions without interface engineering. Using a similar strategy to control the interface, Tsai et al.[9] investigated the impact of a very thin Li- alloyed layer, such as Au. By modifying the surface roughness and by introducing a thin Au layer between Li metal and the solid electrolyte, the interfacial resistance was dramatically reduced, which prevented Li dendrite growth.[10] As an alternative to the Au layer, either a solid electrolyte doped with Nb or a thin layer of Nb deposited at the electrode/electrolyte interface can be used to improve the conductivity locally and thus to decrease the interfacial resistance.[11] Similar results were obtained with a thin layer of Mg,[12] Ge,[13] Li & Na Sn binary alloys.[14] More recently, a new approach emerged in the literature: Since the Li_2CO_3 impurity is detrimental to the cycling performance, researchers tried to modify the lithium carbonate to form Li_3N which is a good Li^+ conductor.[15] The electrochemical results

[a] Dr. G. Ferraresi, Prof. Dr. P. Novák, Dr. C. Villevieille
Paul Scherrer Institute, Electrochemistry Laboratory,
CH-5232 Villigen PSI, Switzerland
E-mail: giulioferraresi@gmail.com
[b] Dr. S. Uhlenbruck, Dr. C.-L. Tsai
Forschungszentrum Jülich GmbH, Institute of Energy and Climate Research
Materials Synthesis and Processing (IEK-1),
52425 Jülich, Germany
[c] Dr. C. Villevieille
Université Grenoble-Alpes, Grenoble INP,
LEPMI Laboratory
1130 Rue de la Piscine, 38402 St Martin d'Hères, France
E-mail: claire.villevieille@gmail.com

Supporting information for this article is available on the WWW under https://doi.org/10.1002/batt.201900173

Special Collection An invited contribution to a Special Collection dedicated to the Symposium on Batteries and Supercapacitors at the E-MRS Spring Meeting 2019

are impressive since the cells can be cycled at 40 °C over 300 cycles and deliver more than 150 mAh/g for the $LiFePO_4$ electrode material. Alternatively, removal of Li_2CO_3 at the surface of the garnet is possible by Ar-etching, as demonstrated by Ferraresi et al. for a thin Si film,[16] leading to promising electrochemical performance. Also, it is possible to proceed with a careful and targeted acid treatment leading to a decrease of the interfacial resistance by a factor of 30, enabling cycling of $LiFePO_4$ and $LiCoO_2$ based cells at 30 °C only.[17] Alternatives based on acid treatment and lithiophilic interface[18] as well as molecular brushes[19] approach were also reported to improve the interface contacts. But still, to date there is less than 200 papers reporting viable electrochemical performance of all-solid-state batteries using a garnet-type solid electrolyte. The issues reported are always the same, i.e. the poor interfacial contact between the solid electrolyte and the respective active material. In most of the cases reported in the literature, insertion based active materials were selected but it is known that, to increase the energy density, alloy/conversion based materials are needed even if they suffer from severe volume changes during the charge/discharge process that could cause mechanical stress and battery failure.[20]

In this context and in order to target bulk-type solid state batteries using insertion/conversion materials we need to optimize the interface. We thus investigated Sn as electroactive model material as it offers a high specific charge as negative electrode material despite of its 300% volume changes during full lithiation.[21] To this point, we investigated two main strategies to prepare the electrode either by a slurry-based process or by thin film sputtering. The former is more appealing, especially for bulk-type batteries, as the engineering is rather simple but it turns out that the garnet is reacting strongly with the solvent used to make the slurry (detectable via X-ray diffraction (XRD) and SEM-cross section experiments), as reported already in the literature, and that the electroactive materials should be in the form of nanoparticles to ensure proper electronic conductivity.[22] By using operando XRD measurements, we found out that Sn particles are properly lithiated during the first cycle. The poor electrochemical performance is due to the large volume changes of Sn during cycling in conjunction with a carbonate rich garnet surface leading to very poor interfacial contact. All of these issues were nicely solved by a proof-of-concept approach based on a pre-lithiated Sn thin film layer, demonstrating significantly enhanced electrochemical performance of all-solid-state cells. However, this approach at the moment is yet only viable for thin film batteries, but it can be used also as a buffer layer to attach properly the bulk electrode and/or Li metal to the solid electrolyte.

2. Results and Discussion

As mentioned in the introduction, one of the weakest points to be solved in the all-solid-state batteries field is the electrode/electrolyte interface.[7c] Its improvement is crucial to ensure stable and reliable electrochemical behavior. To this point, the proper deposition of electrode materials on the surface of the garnet LLZTa electrolyte is of utmost importance and deposition strategies have to be developed. In the present case, the selected electrode candidate for our preliminary investigations is Sn metal, as it has intrinsically good electronic conductivity and relevant understanding of its electrochemical reactivity was already reported for classical Li-ion batteries using conventional organic electrolytes.[23]

2.1. Chemical Interaction Between Sn and LLZTa

The first step was to assess the chemical stability of Sn with LLZTa. Indeed to "attach" properly the Sn electrode to the LLZTa solid electrolyte, the materials (Sn and LLZTa) need to be heated up and the question was if Sn and/or the electrolyte will eventually be deteriorated by this heating process. Thus, we performed in situ temperature X-ray diffraction (XRD), as shown in Figure 1. A 50:50 mixture of Sn and LLZTa powders was thoroughly mixed and placed in an Al_2O_3 crucible in an Anton Paar temperature chamber inside an Empyrean diffractometer from PANalytical. The ISCD card n° 183687 was used for the indexation of LLZTa. We notice a slight shift between the card and the experimental results which is attributed to the misalignment of the zero in the XRD temperature chamber. As can be seen in Figure S1 (Supporting Information) the same sample measured out of the XRD temperature chamber leads to a better matching of the ISCD card. As can be seen, the diffraction peaks of both species (Sn and LLZTa) are partially overlapping at 30.7°, 32°, 44°, and 45° but still we can clearly distinguish them up to 180 °C. At this temperature, there is a small decrease in the peak intensity of Sn reflection with the appearance at 30° of a new small and "amorphized" peak associated to SnO_2 (expected at this temperature). Above this temperature, the reflections associated to Sn start to decrease in intensity after 30 min at 200 °C and they disappear completely after 1 h30 due to the melting of Sn ($T_{melting}$ = 232 °C). The difference between the melting temperature and the one obtained experimentally can be explained by the fact that the measurement was performed under vacuum. After cooling down to 25 °C, the Sn peaks reappear without any

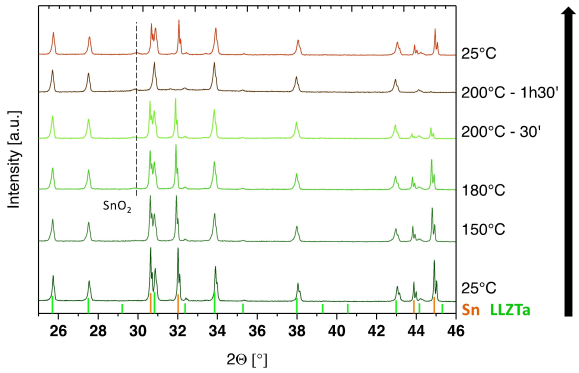

Figure 1. In situ temperature XRD measurement of 50:50 Sn:LLZTa powder mixture. The ICSD card n° 183687 was used to indexed LLZTa.

change compared to the pristine state. This measurement testifies a high chemical stability between Sn and LLZTa (within the XRD detection limit of 0.5% of phase content) at reasonable temperature leading us to continue the investigation of Sn/LLZTa/Li all-solid-state batteries.

2.2. Slurry-Based Sn Composite Electrodes

The first attempt to create a viable cell was to deposit Sn as electroactive material directly on the surface of the LLZTa pellet used also as a separator. In order to create a homogeneous conventional electrode, Sn particles were first dispersed in a N-methyl-pyrrolidone (NMP) solvent with LLZTa solid electrolyte powder (to ensure wettability and proper ionic conductivity), Super C65 as conductive additive, and PVdF binder (40:40:10:10 wt%) under argon atmosphere. The mixture was thoroughly coated on one side of the LLZTa pellets using a brush and the Sn-coated LLZTa pellets were dried at 80 °C under dynamic vacuum to evaporate the solvent and to obtain an electrochemical stack. To evaluate the interface between Sn and the separator (composed of densified pellet of LLZTa), we performed a SEM/EDX analysis on a cross section of the stack as reported in Figure 2. As can be seen, the LLZTa solid electrolyte is located in the lower part of the image, where defined grains of different sizes appear to be properly sintered together (see Supporting Information, Figure S2). The space between the grains of the solid electrolyte is found to be Al-rich which is in agreement with the sintering process since α-Al_2O_3 was used in the initial mixture as sintering additive. The top layer is assigned to the Sn-based electrode mixture deposited on the solid electrolyte, as better visualized in Figure 2b. We can notice here that Al, Ta, La and Zr are not visible in the slurry part which is generally attributed to the set-up and the shadowing effect caused by the EDS detector position. From this morphological analysis, it seems that the electrode mixture is homogeneously coated on the surface of LLZTa pellet, despite a certain roughness of the film. The film seems to be properly attached to the solid-state separator which is a good prerequisite for the electrochemical tests since it is the minimum requirement to ensure a proper Li^+ pathway between the electrode and the electrolyte. Additionally, the EDX mapping analysis, recorded on an extended area at the electrode/electrolyte interface (Figure 2c), reveals the presence of a C-rich layer between LLZTa and the Sn-based electrode. This result indicates that, i) while drying there is a segregation of the carbon particles due to their size and gravity, they sit at the electrode/electrolyte interface and/or ii) there is a thick layer of Li_2CO_3 at the surface of LLZTa pellet, in agreement with our previous results.[16] The Li_2CO_3 layer is coming from the solid electrolyte preparation, sintering process and slicing process, all performed inevitably in the air, even if the exposure time was reduced to the maximum to minimize the thickness of the lithium carbonate. Thus, even if precautions were taken to process the slurry under Ar atmosphere, the lithium carbonate could not be avoided nor reduced.

Additionally, we performed some structural characterization by X-ray diffraction after the slurry deposition/drying process, to check that there is no chemical interaction between the NMP used for the slurry preparation and the solid electrolyte, since we know that there is no degradation between Sn and LLZTa. Unfortunately, and as can be seen in Figure 3, there is a chemical interaction between the NMP solvent and the solid electrolyte. Indeed, an additional phase is detected by XRD appearing at 30° and 34.5° and so far not indexed. None of the known impurities including several quaternary, ternary, binary systems including oxides, carbonates etc, could match the dedicated peaks. Nevertheless, we can speculate that this phase is deriving from the Li-loss and decomposition of LLZTa occurring during the slurry preparation. This phase, due to its poor Li content, could increase the ionic resistance due to its poor Li^+ conductivity.[24]

Nevertheless, despite the presence of this insulating phase and the C-rich layer at the interface between LLZTa/Sn, we decided to test the electrochemical performance of this stack, to define the baseline and to see the impact of a non-optimized electrode engineering.

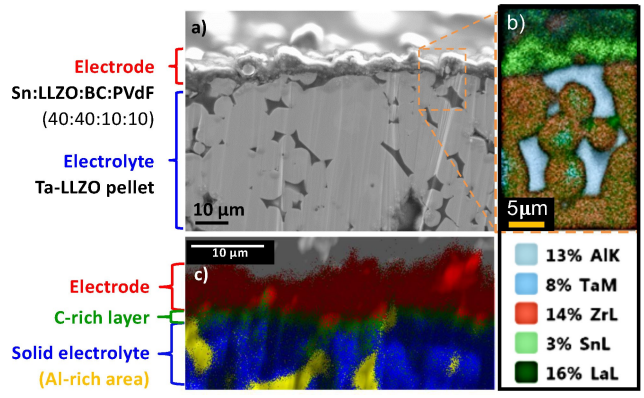

Figure 2. a) Ion-milled cross-section of an Sn slurry-based electrode coated on an LLZTa sample (BC stands for black carbon); b) EDX elemental analysis of the electrode (Sn)/electrolyte (LLZTa) interface; c) EDX mapping analysis of the electrode/electrolyte interface.

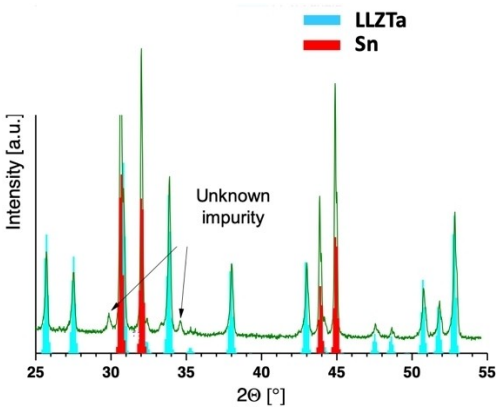

Figure 3. X-ray diffraction pattern of the Sn composite electrode coated on LLZTa sample. The ICSD card n° 183687 was used to indexed LLZTa.

2.3. Electrochemistry of Slurry-Based Sn Electrodes

Sn-coated LLZTa half-cells were assembled under Ar atmosphere by pressing a thin Li foil on the uncoated side of the LLZTa pellet and maintained under constant pressure during the electrochemical measurement performed in a Swagelok-type cell. Due to the expected high interfacial resistance, the electrochemical performance were measured at $T = 100\,^{\circ}C$. The electrochemical investigations were conducted using a galvanostatic cycle coupled to a potentiostatic step applied at the cut-off potentials (so called CCCV protocol for constant current-constant voltage). As the Sn electroactive material is known for its poor Li diffusion especially in big particles (core-shell process),[20a] we tested two different Sn particle sizes, 44 μm and 100 nm,[25] both reported in Figure 4. For the Sn nanoparticles, it is well known that the surface is covered by a native surface layer of SnO_2. In a similar study, we performed XPS on this sample which reveals the presence of SnO_2 but also of Sn^0 indicating that the thickness of the native layer should be less than 8 nm (detection limit of the XPS machine). Thus, only a small part of the CV can be attributed to SnO_2 (less than 10%). Cyclic voltammogram of the Sn micro-sized particles (44 μm) as well as the derivative curves of Sn nano-sized Sn are displayed in the Supporting Information (Figure S3).

Figure 4 a reports the initial four cycles using Sn (44 μm) particles. The first lithiation step consists of a sloping potential plateau below 0.5 V vs. Li^+/Li, corresponding to nearly 800 mAh/g (close to the theoretical specific charge of ca. 990 mAh/g). During the first delithiation, the retrieved specific charge was limited to 50 mAh/g (only 30 mAh/g without the potentiostatic step). These poor electrochemical results can be explained by several factors such as i) the poor interfacial contact between the electrode and the solid electrolyte (separator), ii) phases generated at the interface between Sn/LLZTa creating an insulating layer (Li_2CO_3 and unknown impurities),[22] and iii) the lithiation of the Sn particles that can generate volume change of more than 300% leads to particles' fracture and most probably "film pilling of" and particles disconnection, as already reported.[26] As a consequence, the following cycles are presenting very poor electrochemical performance since we were unable to exceed 15 mAh/g in galvanostatic mode, corresponding to less than 2% of the expected theoretical specific charge. As a low charge can still be obtained from the potentiostatic steps, we can also add a kinetics limitation due to i) bad contact between the active materials and the solid electrolyte and ii) carbon black segregation hindering proper electronic pathway, both of them generating very high polarization. Thus, and based on the aforementioned observations, we made another test using smaller Sn particles (100 nm) with the hope to tackle or at least buffer the pre-cited issues. Figure 4b shows the initial four cycles of the Sn/LLZTa/Li cell in CCCV mode, where two main regions can be distinguished:

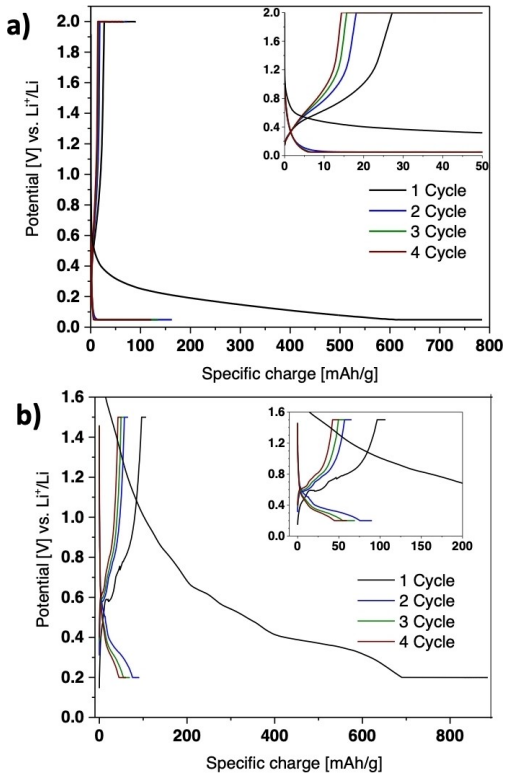

Figure 4. Electrochemical cycling of Sn composite electrodes coated on LLZTa, vs. Li metal, cycled at 100 °C (C/50 rate): a) Sn micro-sized particles (44 μm); b) Sn nano-sized particles (100 nm).

- From 2.0 V down to 0.8 V vs. Li^+/Li, Sn is not electrochemically active, therefore no electrochemical activity is expected. Additionally, since we are not in conventional Li-ion batteries, we are not expecting any classical solid-electrolyte interphase (SEI) formation even if to date we cannot fully exclude side reactions to happen in this region. Nevertheless, there is a detectable electrochemical activity above 0.8 V vs. Li^+/Li during the first lithiation. This activity could be attributed to the electrochemical reactivity of the surface native SnO_2 layer. This particular phenomenon was not observed for bigger Sn particles which can be explained by the proportion of Sn/SnO_2. Indeed, when the particles are large (44 μm), SnO_2 is only present at the outer surface (couple of nm) but the ratio Sn/SnO_2 makes the contribution of SnO_2 negligible whereas when the Sn particles are in the nanometer range, the contribution of SnO_2 is clearly visible as in the present case. Thus, in this potential range, we supposed that SnO_2 is reduced to another phase that could be reduced and attributed to Li_2SnO_3 as analogy with liquid electrolyte measurement or to Li_2SnO_2 as we have less oxygen in this system than in liquid organic electrolyte.[27]
- From 0.8 V down to 0.2 V vs. Li^+/Li, three defined potential plateaus at 0.63 V, 0.52 V, and 0.39 V vs. Li^+/Li are observed and are related to the formation of several Li–Sn alloys, as described in the literature (LiSn, Li_2Sn_5, Li_7Sn_5, etc., see Operando XRD section below). At the end of the full lithiation, the cell delivers a specific charge of ca. 900 mAh/g (with 200 mAh/g coming from the potentiostatic step) which is a very promising value for the lithiation of Sn. During the first delithiation, the galvanostatic curve turns smooth since no potential plateau is distinguishable and the polarization is very high leading to delivering a specific charge close to

100 mAh/g. Again, the poor electrochemical performance can be attributed to the insufficient electrode engineering and a less suitable deposition technique. The further lithiation cycles show a drop of the specific charge down to 50 mAh/g, mainly coming from the electrochemical activity observed at 0.52 V and 0.39 V vs. Li^+/Li, indicating still a minor electrochemical activity of Li with Sn.[28]

As seen, the electrochemical investigation shows poor electrochemical performance after the first lithiation. Several reasons were already discussed and come from the suboptimal engineering of the electrode and the poor contact at the electrode/electrolyte interface. Indeed, LLZTa is covered by Li_2CO_3 at its surface which hinders a good contact with the electroactive materials. Since we did not use any sintering step that would have drastically damaged the binder used in the composite electrode, the contact between SE and Sn is not optimal leading to lower the ionic transport in the electrode. Furthermore, Sn is known to react through an alloying reaction path generating very large volume changes which creates additional stresses/fractures leading to poor contact. By replacing Sn microparticles with Sn nanoparticles, we managed to improve the electrochemical performance of the cell indicating also that the engineering should not be only focusing on the intimate mixture of several components but also on tuning the granulometry of the electroactive materials. In both cases, the irreversibility observed after the first lithiation reveals a severe hindrance in the delithiation of Li–Sn alloys caused also by the slurry-based electrode composite preparation, which creates a porous network limiting the interfacial contact and further worsens by the presence of the pyrochlore phase from the side reactions of LLZTa during the electrode preparation.

2.4. Operando XRD Characterization of 100 nm Sn/LLZTa

As we identified several potential plateaus during the first lithiation of Sn/LLZTa/Li stack and obtained a reasonable specific charge, we performed a structural investigation using operando XRD to determine the structural nature of the several potential plateaus, most probably linked to Li_xSn alloys formed normally upon cycling of Sn vs Li. As already discussed in respect to the XRD pattern reported in Figure 3, the distinction between LLZTa and Sn^0 pattern is challenging due to the overlap of the peaks at 30.35° and 31.75° but still some information can be extracted along cycling, especially for the development of new phases. Figure 5, complemented by Figure S4 (Supporting Information), shows the operando XRD measurement of the 100 nm Sn composite electrode coated on the LLZTa pellet. As anticipated, the Sn^0 peaks are hidden by the ones of LLZTa, therefore their disappearance could not be formally investigated quantitatively. However, it was easy to evidence the presence of the Li–Sn alloys due to the appearance of a peak at 35°, matching the expected Li_2Sn_5 phase. This phase is further converted into a LiSn phase before the end of lithiation, as confirmed by the appearance of three Bragg diffraction peaks at 35.5°, 36.8°, and 38°, although the

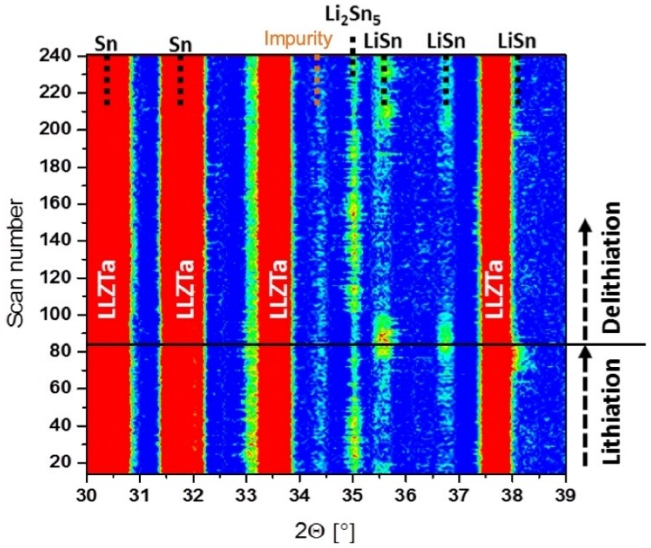

Figure 5. Contour plot representation of an operando X-ray diffraction measurement of an Sn composite electrode coated on LLZTa and cycled vs. Li metal at 90 °C in the potential range 0.2–1.6 V vs. Li^+/Li at C/50 rate. The ICSD card n° 183687 was used to indexed LLZTa, the ICSD card n° 00-004-0673 was used for Sn indexation, the card n° 01-074-0561 for Li_2Sn_5 and the card n° 00-029-0839 for LiSn.

latter was partially overlapping with the LLZTa diffraction peak at 37.8°. Formation of a higher lithiated Li_xSn_y alloy could not be directly proven due to the peak overlapping at 38°. Nevertheless, the stable peak intensity of the LiSn phase coupled to i) the very high overpotential observed electrochemically and ii) the contribution of the potentiostatic step, would not suggest further lithiation. During delithiation, the LiSn phase disappears in parallel to the re-appearance of the Li_2Sn_5 phase at 35°. This latter phase was however not disappearing at the end of delithiation, confirming the high irreversibility already observed during the first cycle shown in Figure 4 and the poor electronic/ionic conductivity of the system.

Although the difficulties encountered with the overlap of several peaks, we observed the alloying reaction of Sn^0 with Li, showing the partial reversible electrochemical activity of the stack. These results demonstrate the need of a better approach to improve the electrode/electrolyte contact.

2.5. Sn Thin Film Electrodes on the Garnet LLZTa Solid Electrolyte

As a proof of concept, we investigated the possibility to deposit Sn thin films on LLZTa solid electrolyte pellet at room temperature using a sputtering technique. The surface-edge of the LLZTa pellets was covered by a circular shadow mask to allow only a ~9.5 mm Sn-coated surface. Prior to each deposition, the LLZTa surface was exposed for 30 s to Ar^+ etching to remove the lithium carbonate naturally covering the surface of the LLZTa pellet.[16]

As can be seen from Figure 6, the 50 nm Sn film shows the typical island morphology for Sn as already reported in the literature.[29] The film appears homogeneously covering the surface of LLZTa and the diameter of the islands is in the range 50–150 nm.

As for the previous slurry-based deposition attempts, we assessed the electrochemical performance of the Sn thin film stack by performing CV measurements and galvanostatic cycling in half-cell configuration. Figure 7a shows the first CV cycle at a scan rate of 20 μV/s, where the cathodic scan reveals initial electrochemical activity below 0.7 V vs. Li^+/Li and a dominant reduction activity at ca. 0.3 V vs. Li^+/Li and 0.25 V vs. Li^+/Li, corresponding to alloying reactions between Li and Sn. During the anodic scan, the current response is negative up to 0.35 V vs. Li^+/Li (which indicates incomplete lithiation at the given scan rate), while above it two major oxidation processes are observed at 0.45 V vs. Li^+/Li and 0.6 V vs. Li^+/Li. An additional broad peak is observed at higher potentials in the range from 0.75 V to 1.3 V vs. Li^+/Li.

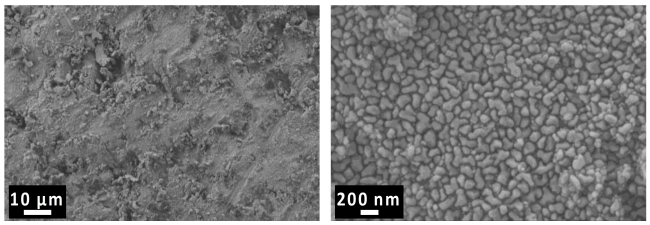

Figure 6. SEM images of the 50 nm Sn thin film deposited on 500 μm garnet LLZTa pellet.

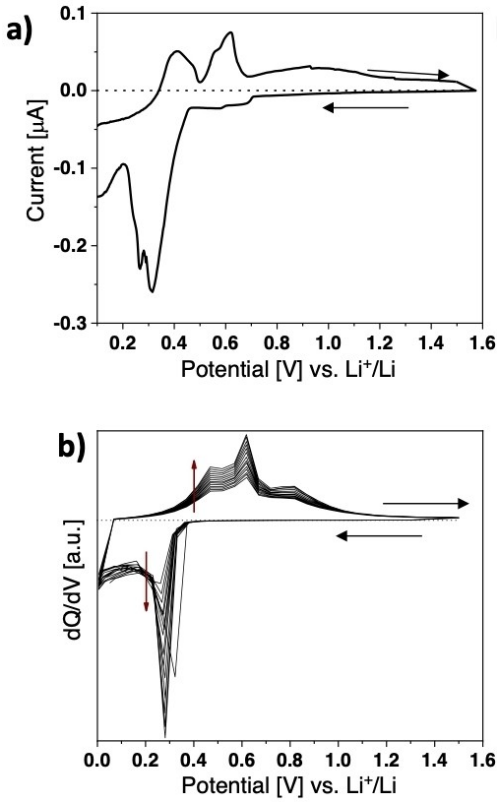

Figure 7. Electrochemical cycling of a 50 nm Sn thin film deposited on LLZTa solid electrolyte, vs. Li metal, at T = 100 °C: a) Cyclic voltammetry performed at a scan rate = 20 μV/s in the range 0.1 V–1.6 V vs. Li^+/Li; b) Derivative curves of galvanostatic cycling measurement at C/100 rate in the range 5 mV–1.6 V vs. Li^+/Li.

Similar electrochemical response is observed in Figure 7b showing the derivative curves of the galvanostatic cycling, although in this case the peak intensities are lower during initial cycles and the retrieved specific charge (less than 100 mAh/g) is much lower than the theoretical value for Sn. Increasing the cycle number, the peak intensity increases continuously (Figure 7b), suggesting that there is a kind of activation mechanism,[30] i.e., a hindrance to lithiate fully the Sn thin film initially. This effect might be caused by i) the initial poor Sn/LLZTa interface contact, which becomes more stable as soon as the film begins to get lithiated, ii) a conductivity-based hindrance avoiding lithiation of the stack at the applied C-rate, and iii) the stress caused by successive lithiation/delithiation is opening new Li pathways leading to make accessible some Sn particles so far disconnected. Nevertheless, the severe volume change of Sn could be also too detrimental for long-term cycling. Thus, we looked for an alternative to avoid the first large volume changes by pre-lithiating Sn.

2.6. Chemical Pre-Lithiation and Electrochemistry of Li_xSn Thin Films

Based on the above-revealed limitations, we decided to chemically pre-lithiate the 50 nm Sn film to avoid the initial large volume change. To this point, we directly contacted Li metal with the 50 nm Sn thin film at $T = 180–200$ °C under Ar atmosphere, as shown in Figure 8. The Li amount was chosen to ensure the full lithiation of the Sn thin film, and thus was slightly in excess. In a few minutes, the light-grey film turns darker due to the Li^+ diffusion inside the Sn thin film.

Once the film completely turned black in less than 10 min, the Sn thin film was successively cooled down and investigated electrochemically in half-cell configuration, as reported in Figure 9. After cell assembly, the open circuit potential (OCP) was found to be 40 mV vs. Li^+/Li, in agreement with a Li_xSn_y alloy. As the potential is close to 0 V vs. Li^+/Li, it indicates that the amount of Li in Sn is high, most probably higher than 3. Additionally, in the present case the OCV potential is ca. 50 mV vs. Li^+/Li indicating that we are very close to the maximum alloy materials Li_7Sn_2 ($Li_{22}Sn_5$ being obtained at potential close to, or even below 0 V vs. Li^+/Li). Finally, the delithiation profile is matching the one reported in the literature.[31] Figure 9a

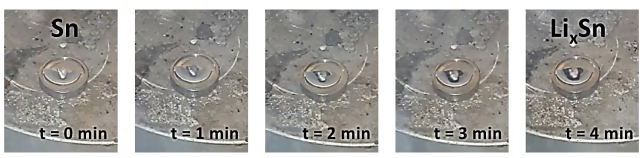

Figure 8. Image sequence of the formation of Li_xSn alloy upon chemical reaction during heating process in an Ar-glovebox.

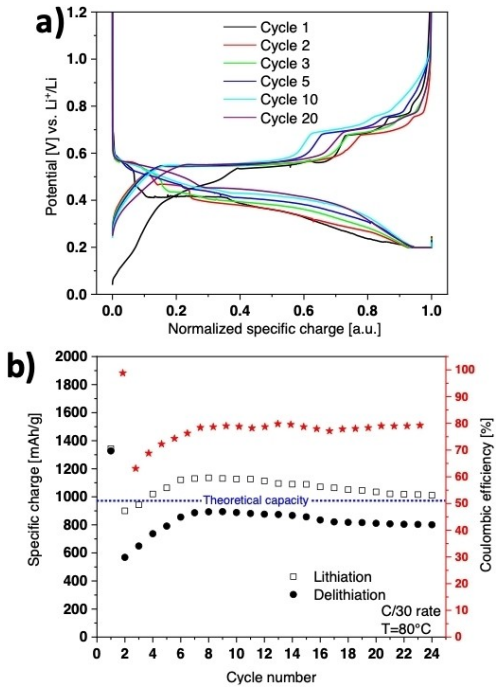

Figure 9. a) Normalized galvanostatic potential profiles of selected cycles of chemically lithiated 50 nm Sn thin film on LLZTa vs. Li metal at C/30 rate (80 °C); b) specific capacity retention for 25 cycles of this system.

shows the galvanostatic potential profile of selected cycles after normalization of the specific charge. As can be seen, the first delithiation reveals the presence of multiple potential plateaus at 0.2 V, 0.45 V, 0.53 V, 0.62 V, and 0.72 V vs. Li^+/Li, all of them corresponding to an alloy Li_xSn_y. The two potential plateaus below 0.5 V vs. Li^+/Li were not visible in the previous experiments (Figure 4, Sn slurry-based electrode), while the three potential plateaus above 0.5 V vs. Li^+/Li match well the values reported above. This behavior indicates most probably that, in the previous cases (slurry based and non-pre-lithiated Sn electrodes), the interfacial resistance at the solid/solid interface was so high that it resulted in a very high overpotential hindering the last Sn–Li alloy process, the one creating phases that are richer in Li and responsible of most of the specific charge gathered. On the following lithiation, minor electrochemical activity is observed at 0.58 V and 0.46 V vs. Li^+/Li and a dominant potential plateau appears at 0.4 V vs. Li^+/Li until the cut-off potential of 0.2 V vs. Li^+/Li indicating that Sn can be "easily" re-lithiated. This result is in agreement with the stress caused by the lithiation/delithiation. Indeed, when we start from the pre-lithiated pristine materials, Li can be easily extracted from the materials as it is less stressful for the electrode. Then when inserting back the Li, there is also less stress caused because the material does not fully shrink and offers "voids" to accommodate the Li ions. The second delithiation shows a decreasing electrochemical activity in the region below 0.5 V vs. Li^+/Li and an unvaried electrochemical activity above 0.5 V vs. Li^+/Li. Similarly, during the lithiation step the electrochemical response shows activity at similar potentials with an increasing contribution of the reactions at 0.58 V and 0.46 V vs. Li^+/Li. The following delithiation and lithiation cycles do not show the appearance of additional electrochemical processes but they reveal the increase of the contribution from the reactions above 0.6 V vs. Li^+/Li, until the 10th cycle. Similarly, during lithiation the process above 0.45 V vs. Li^+/Li rises also after 10 cycles. Surprisingly, we can see a strong decrease of the overpotential during cycling indicating probably a more favorable resistance when compared to the first cycle. Also, the changes noticed in the Li pathway and the length of some potential plateaus might indicate that alternative Li–Sn compositions are generated during cycling and/or that some Sn particles are getting accessible after few cycles, as already reported in the literature.

This impact on the specific charge is better seen in Figure 9b. The first cycle shows an initial specific charge above 1300 mAh/g with high Coulombic efficiency (>98%). This specific charge, above the theoretical one for Sn, is most probably caused by side reactions including the possible deposition of Li metal leading to extra capacity. The second cycle shows a drop in specific charge to 570 mAh/g. This value rises constantly up to the 10th cycle, where it reaches almost 900 mAh/g with a Coulombic efficiency (CE) of around 82%. This behavior appears as an activation process from the 2nd to the 10th cycle. After 25 cycles the specific charge is stabilized around 800 mAh/g, showing excellent cycling performance for an all-solid-state cell using garnet solid-electrolyte even if the measurement was performed at high temperature T = 80 °C. The poor CE can be explained by side reactions coming from the decomposition of surface layer materials (carbonates, hydroxides, et), but also by the volume changes and particles' disconnection occurring during cycling. These results show the significant improvement in the cycling performance obtained by using the 50 nm, lithiated Sn thin films alternatively to Sn composite electrodes, even if we know that the thin films are only used here as a proof of concept. Despite the chemical lithiation, it seems that Sn undergoes an activation process that can be caused by:

- Intrinsic effects induced by the LLZTa electrolyte;
- diffusion kinetics;
- possible electrochemical interaction of Sn with LLZTa, creating a stable interface or even reacting and/or forming an interfacial conductive layer; and
- presence of undesired species at the interface, such as LiOH and/or Li_2CO_3, which get decomposed upon cycling, reducing the interface resistance.

3. Conclusions

With this work, we demonstrated the importance of the electrode engineering to obtain a meaningful electrochemical response. In the case of all-solid-state batteries the requirements for the electrode preparation are very different from the ones typical for conventional Li-ion batteries. In all-solid-state batteries, the primary challenge is the contact between the electroactive materials and the solid electrolyte. The need for a proper contact between two solid materials prohibited then

the usage of a standard slurry-based electrode preparation as demonstrated here via the problems to delithiate such electrodes due to the high interfacial polarization. To optimize the contact between the electroactive materials and the electrolyte at the interface, we opted for a proof-of-concept approach of thin film deposition but here, the cells suffered from the intrinsic alloying nature of the electroactive material, Sn, well known to suffer from very large volume changes once alloying and thus creating particles disconnection. To overcome this last issue, we proposed here to pre-lithiate the Sn thin film which finally lead to a demonstration of a proper cycling stability with Coulombic efficiency $>80\%$ and specific charge higher than 800 mAh/g. These results, despite being obtained on thin films, are promising as they demonstrate that it is possible to properly cycle all-solid-state cells using garnet solid electrolyte, provided proper electrode engineering. Our approach here can lead also to use Sn as a buffer layer between the solid electrolyte and the Li metal, to improve the interfacial resistance. For sure, additional research is needed in this area to optimize the interfacial contact but also to find a methodology that will allow cycling practical bulk type electrode materials.

Experimental Section

Synthesis, processing, and sintering of garnet solid electrolyte

The raw Ta-substituted LLZ (LLZTa) powder was initially synthesized by solid-state reaction.[9] Shortly, the raw materials used for the synthesis were $LiOH{\cdot}H_2O$ 99.99% with a 20% wt. excess (Panreac), Ta_2O_5 99,99% (Infranet), γ-Al_2O_3 with 5% excess (Infranet), ZrO_2 99+% (Alfa), and La_2O_3 (Alfa). La_2O_3 underwent a pre-treatment step by heating up at 900 °C to limit H_2O absorption and then it was quickly stored under dry atmosphere (glovebox or desiccator) to prevent further reaction with moisture. The powder was placed in a 13 mm evacuable pellet press die (Specac) by uniaxial pressing with 10 kN for five minutes and the obtained rod was placed on a MgO plate prior to its insertion inside a covered alumina crucible for sintering at 1175 °C for 5 h in air with a heating ramp rate of 5 °C/min followed by natural cooling. MgO plate acts as buffer to avoid direct contact between alumina and LLZTa, as Al could be transferred to the pellet at such temperature creating uncontrolled stoichiometric difference. As a consequence of the sintering, the final diameter of the compressed LLZTa samples shrinks down to ~11 mm. The rods (~2 cm in height) were finally cut in several pellets with a diamond-wire tool (to the thickness of ~600 μm. Both surfaces of the LLZTa pellets were manually polished with SiC grinding papers (Buehler ITW) having a grit size of 320, 400, 600, 1000 to obtain the targeted thickness and a mirror-like surface. Between each process the samples were stored in dry atmosphere to reduce the exposure to air/moisture.

Electrochemical tests

The all-solid-state cells (SSC) were assembled in a Swagelok-type hardware. The advantage of Swagelok cells for SSC testing is the possibility to adjust the internally applied pressure according to the overall height of the solid-state stack. As the measurements are carried at high temperature (up to 120 °C), the Swagelok-type cells were internally insulated by using PET films (Mylar) and PTFE rings, which are ideal electron insulators and gas tight gaskets. For the electrochemical characterization of the SSCs, a special treatment was applied to ensure the Li metal/LLZTa adhesion. One-side of the LLZTa pellet was coated with 5 nm Au prior to the Li foil deposition. To this point, the Li metal was heated at 200 °C for 30 min inside the glovebox to form a Li_xAu interlayer. Copper foils as current collectors were applied on both sides to provide better electronic pathway. Before any electrochemical test, the assembled Swagelok-type cells were rested at 80 °C overnight, re-tightened and electrochemically cycled in the desired potential range. All the electrochemical measurements were conducted with a VMP-3 multi-channel potentiostat/galvanostat or VMP-300 multi potentiostat (Bio-Logic). The test cells were always connected with co-axial cables in a temperature-controlled chamber.

X-ray diffraction

The measurements were performed on a PANalytical Empyrean diffractometer with a Cu Kα radiation in Bragg-Brentano geometry. Two types of measurements were conducted: XRD reflection coupled with cell cycling in operando mode and powder XRD reflection at different temperatures (Anton Paar HTK 1200N). For the former, operando measurements were conducted using a specifically designed cell, described in Ref. [32]. To ensure X-ray transparency during the measurement, Be window was selected and an external resistance heating connected to a temperature controller was bound externally to the cell to perform the measurement at elevated temperature (tested up to 90 °C). For the powder XRD, a typical measurement was conducted by placing the sample into a crucible which was inserted in the heating chamber. An XRD pattern was measured at RT and subsequently the sample was heated up to a specific temperature, rested for at least 30 min, and XRD patterns were recorded before moving to the next temperature. After having reached the highest temperature desired, the sample was cooled down to RT and a final XRD pattern was acquired.

Scanning electron microscopy

SEM measurements were performed with a Carl Zeiss Ultra55 scanning electron microscope, varying the acceleration voltage of the electron gun in the range 3–15 kV. This instrument was also equipped with an energy dispersive X-ray analysis detector (EDX).

Ion milling cross-section

Cross-sectioning cuts of the samples were performed using an IM4000plus ion-milling system (Hitachi) with Ar^+ beam. The working principle is the same as of a sputtering machine, except that the sample is partially masked and a low energy ion beam is focused on a definite area of the sample, orthogonal to the beam flux, to ablate locally the material. For garnet LLZTa solid electrolyte, an optimum condition for a 0.6–1 cm thick sample was found by applying a continuous beam irradiation of 4.0 kV with 30 reciprocations/min and $\pm 30°$ swing for 8–12 h.

Thin-film deposition

The samples were deposited using Ar as a sputtering gas at a flow rate of 5 sccm which results in a stable Ar- pressure of $\sim 4\times 10^{-3}$ mbar during deposition. A base pressure of $\sim 1\times 10^{-6}$ mbar was achieved prior to deposition. A Sn target of 75 mm diameter was sputtered using a power of 100 W. The obtained deposition rate was 3.5 nm/s. The distance between the target surface and the

sample was fixed to 80 mm. After deposition, the Sn films were immediately stored under Ar atmosphere to limit the inevitable native oxide layer.

Acknowledgements

We are thankful to Mr. M. Horisberger (LMN, PSI) for the Sn thin film deposition on the garnet electrolyte. Financial support by Helmholtz Gemeinschaft Deutscher Forschungszentren e.V. under grant "Speicher und Vernetzte Infrastrukturen", Helmholtz Institute Münster (HI MS), and by Bundesministerium für Bildung und Forschung (Federal ministry of education and research), Germany, under projects No. 13N9973 and 03X4634C is gratefully acknowledged. The authors are responsible for the content.

Keywords: Li-ion batteries · solid-state batteries · garnet electrolyte · operando XRD · Sn negative electrode

[1] a) Y. Ding, Z. P. Cano, A. Yu, J. Lu, Z. Chen, *Electrochem. Energy Rev.* **2019**, *2*, 1–28; b) M. Winter, B. Barnett, K. Xu, *Chem. Rev.* **2018**, *118*, 11433–11456; c) M. Li, J. Lu, Z. Chen, K. Amine, *Adv. Mater.* **2018**, *30*, 1800561.
[2] a) M. R. Palacín, *Chem. Soc. Rev.* **2018**, *47*, 4924–4933; b) K. Liu, Y. Liu, D. Lin, A. Pei, Y. Cui, *Sci. Adv.* **2018**, *4*, eaas9820.
[3] F. Zheng, M. Kotobuki, S. Song, M. O. Lai, L. Lu, *J. Power Sources* **2018**, *389*, 198–213.
[4] a) K. H. Park, Q. Bai, D. H. Kim, D. Y. Oh, Y. Zhu, Y. Mo, Y. S. Jung, *Adv. Energy Mater.* **2018**, *8*, 1800035; b) J. Lau, R. H. DeBlock, D. M. Butts, D. S. Ashby, C. S. Choi, B. S. Dunn, *Adv. Energy Mater.* **2018**, *8*, 1800933.
[5] a) J. C. Bachman, S. Muy, A. Grimaud, H.-H. Chang, N. Pour, S. F. Lux, O. Paschos, F. Maglia, S. Lupart, P. Lamp, L. Giordano, Y. Shao-Horn, *Chem. Rev.* **2016**, *116*, 140–162; b) Y. Zhu, X. He, Y. Mo, *ACS Appl. Mater. Interfaces* **2015**, *7*, 23685–23693.
[6] Q. Liu, Z. Geng, C. Han, Y. Fu, S. Li, Y.-b. He, F. Kang, B. Li, *J. Power Sources* **2018**, *389*, 120–134.
[7] a) X. Yu, A. Manthiram, *Energy Environ. Sci.* **2018**, *11*, 527–543; b) Y. Shao, H. Wang, Z. Gong, D. Wang, B. Zheng, J. Zhu, Y. Lu, Y.-S. Hu, X. Guo, H. Li, X. Huang, Y. Yang, C.-W. Nan, L. Chen, *ACS Energy Lett.* **2018**, *3*, 1212–1218; c) J. Dai, C. Yang, C. Wang, G. Pastel, L. Hu, *Adv. Mater.* **2018**, *30*, 1802068.
[8] J. van den Broek, S. Afyon, J. L. M. Rupp, *Adv. Energy Mater.* **2016**, *6*, 1600736.
[9] C.-L. Tsai, V. Roddatis, C. V. Chandran, Q. Ma, S. Uhlenbruck, M. Bram, P. Heitjans, O. Guillon, *ACS Appl. Mater. Interfaces* **2016**, *8*, 10617–10626.
[10] C.-L. Tsai, Q. Ma, C. Dellen, S. Lobe, F. Vondahlen, A. Windmüller, D. Grüner, H. Zheng, S. Uhlenbruck, M. Finsterbusch, F. Tietz, D. Fattakhova-Rohlfing, H. P. Buchkremer, O. Guillon, *Sustainable Energy Fuels* **2019**, *3*, 280–291.
[11] T. Kato, T. Hamanaka, K. Yamamoto, T. Hirayama, F. Sagane, M. Motoyama, Y. Iriyama, *J. Power Sources* **2014**, *260*, 292–298.
[12] K. Fu, Y. Gong, Z. Fu, H. Xie, Y. Yao, B. Liu, M. Carter, E. Wachsman, L. Hu, *Angew. Chem. Int. Ed.* **2017**, *56*, 14942–14947.
[13] W. Luo, Y. Gong, Y. Zhu, Y. Li, Y. Yao, Y. Zhang, K. Fu, G. Pastel, C.-F. Lin, Y. Mo, E. D. Wachsman, L. Hu, *Adv. Mater.* **2017**, *29*, 1606042.
[14] C. Wang, H. Xie, L. Zhang, Y. Gong, G. Pastel, J. Dai, B. Liu, E. D. Wachsman, L. Hu, *Adv. Energy Mater.* **2018**, *8*, 1701963.
[15] H. Xu, Y. Li, A. Zhou, N. Wu, S. Xin, Z. Li, J. B. Goodenough, *Nano Lett.* **2018**, *18*, 7414–7418.
[16] G. Ferraresi, M. El Kazzi, L. Czornomaz, C. L. Tsai, S. Uhlenbruck, C. Villevieille, *ACS Energy Lett.* **2018**, *3*, 1006–1012.
[17] H. Huo, Y. Chen, N. Zhao, X. Lin, J. Luo, X. Yang, Y. Liu, X. Guo, X. Sun, *Nano Energy* **2019**, *61*, 119–125.
[18] a) Y. Ruan, Y. Lu, X. Huang, J. Su, C. Sun, J. Jin, Z. Wen, *J. Mater. Chem. A* **2019**, *7*, 14565–14574; b) Y. Lu, X. Huang, Y. Ruan, Q. Wang, R. Kun, J. Yang, Z. Wen, *J. Mater. Chem. A* **2018**, *6*, 18853–18858.
[19] W. Li, C. Sun, J. Jin, Y. Li, C. Chen, Z. Wen, *J. Mater. Chem. A* **2019**, *7*, 27304–27312.
[20] a) X. Wu, J. Billaud, I. Jerjen, F. Marone, Y. Ishihara, M. Adachi, Y. Adachi, C. Villevieille, Y. Kato, *Adv. Energy Mater.* **2019**, *9*, 1901547; b) S.-H. Yu, X. Feng, N. Zhang, J. Seok, H. D. Abruña, *Acc. Chem. Res.* **2018**, *51*, 273–281.
[21] M. N. Obrovac, V. L. Chevrier, *Chem. Rev.* **2014**, *114*, 11444–11502.
[22] R. H. Brugge, A. K. O. Hekselman, A. Cavallaro, F. M. Pesci, R. J. Chater, J. A. Kilner, A. Aguadero, *Chem. Mater.* **2018**, *30*, 3704–3713.
[23] a) N. Oehl, G. Schmuelling, M. Knipper, R. Kloepsch, T. Placke, J. Kolny-Olesiak, T. Plaggenborg, M. Winter, J. Parisi, *CrystEngComm* **2015**, *17*, 8500–8504; b) K. J. Rhodes, R. Meisner, M. Kirkham, N. Dudney, C. Daniel, *J. Electrochem. Soc.* **2012**, *159*, A294–A299.
[24] a) C. Loho, R. Djenadic, M. Bruns, O. Clemens, H. Hahn, *J. Electrochem. Soc.* **2017**, *164*, A6131–A6139; b) G. Larraz, A. Orera, M. L. Sanjuán, *J. Mater. Chem. A* **2013**, *1*, 11419–11428.
[25] L. O. Vogt, C. Marino, C. Villevieille, *Chimia* **2015**, *69*, 729–733.
[26] B. Wang, B. Luo, X. Li, L. Zhi, *Mater. Today* **2012**, *15*, 544–552.
[27] G. Ferraresi, C. Villevieille, I. Czekaj, M. Horisberger, P. Novak, M. El Kazzi, *ACS Appl. Mater. Interfaces* **2018**, *10*, 8712–8720.
[28] M. Winter, J. O. Besenhard, *Electrochim. Acta* **1999**, *45*, 31–50.
[29] E. Bauer, in *Zeitschrift für Kristallographie – Crystalline Materials, Vol. 110*, **1958**, p. 395.
[30] a) L. O. Vogt, M. El Kazzi, E. J. Berg, S. P. Villar, P. Novak, C. Villevieille, *Chem. Mater.* **2015**, *27*, 1210–1216; b) L. O. Vogt, C. Villevieille, *J. Electrochem. Soc.* **2016**, *163*, A1306–A1310.
[31] F. Yin, X. Su, Z. Li, J. Wang, *J. Alloys Compd.* **2005**, *393*, 105–108.
[32] P. Bleith, H. Kaiser, P. Novak, C. Villevieille, *Electrochim. Acta* **2015**, *176*, 18–21.

Manuscript received: November 5, 2019
Revised manuscript received: February 14, 2020
Accepted manuscript online: February 14, 2020
Version of record online: March 6, 2020